DOI: 10.13009/EUCASS2022-4480

Control strategies comparison and performance evaluation for a reusable VTVL platform based on a rocket engine

AFILIPOAE Tudorel-Petronel, NECULĂESCU Ana-Maria
National Institute for Aerospace Research 'Elie Carafoli' – INCAS, Iuliu Maniu Blvd., 220, sector 6, 061126, Bucharest, Romania,
{afilipoae.tudorel, neculaescu.ana} @incas.ro

SIMPLICIO Pedro, BENNANI Samir
European Space Agency, Keplerlaan 1, NL-2200 AG Noordwijk, The Netherlands,
{pedro.simplicio, samir.bennani} @esa.int

STRAUCH Hans
3db-consult - PO Box 28219 Bremen, Germany, hans.strauch@3db-consult.de

Abstract
In the frame of a reusable VTVL platform development with the purpose of researching novel techniques for approach and landing and system testing, a full blown 6-DOF flight simulator was developed to serve as the core simulation environment for the ADAMP project. The objective of ADAMP project is to develop and test novel autonomous retro-propulsive landing strategies and within this paper, comparative GNC development results for the reusable platform are presented.
The Flight Simulator is used for the implementation and testing of different control strategies for the ADAMP platform and, in this article, two control strategies for the reusable VTVL platform are developed, discussed and compared.
The first one relying on a robustly self-scheduled structured H-infinity optimization strategy for the translational, pitch and roll motions, while the second control strategy relies on a nonlinear sliding mode strategy.
For the linear design strategy stability robustness and performance robustness analyses are provided in both frequency domain and time domain. While the comparative analyses campaigns rely on high fidelity 6-DOF Monte-Carlo simulations. The simulations reveal the trade-off between in robustness and performance in both cases. We conclude with design considerations and lessons learned to this application on the mechanization of both control methodologies.

1 Introduction

The international trend in space business is proving the ability to reuse space technology and this can be easily seen in the space exploration and transportation scene with all major players allocating a lot of effort to demonstrate all these technologies which will lead to profitability on the long run.
In this context, the Ascent and Descent Autonomous Manoeuvrable Platform (ADAMP) initiative is undertaken as a development by the National Institute for Aerospace Research "Elie Carafoli" – INCAS Romania with the support of the European Space Agency (ESA) through the General Support Technologies Program (GSTP) and the Romanian Space Agency (ROSA). ADAMP initiative addresses one key element for space technology innovation, which is rapid turnaround and low-cost system testing. ADAMP will serve as an in-flight testing platform for several control strategies, for real time autonomous and fuel optimal guidance strategies, for safe precision landing innovative techniques, as well as hardware components such as sensors, computers and on-board cameras.
ADAMP activity consists of the development of a reusable test platform through building an experimental Vertical Take-Off and Landing (VTVL) platform accompanied by the corresponding facilities, personnel and procedures. This will allow to host testing and verification and validation campaigns for other companies and institutes in a fast and reliable manner, as well as to readily tailor experiments for bigger space programs. ADAMP builds up on the heritage of the previous vehicle developed by INCAS, Demonstrator for Technologies Validation (DTV) [1]. ADAMP platform 1st fully integration tether testing flight is planned for the end of 2022.
In the frame of the ADAMP project, a Flight Simulator consisting of guidance and control algorithms as well as a moderate fidelity plant model within MATLAB-Simulink environment has been developed at INCAS. This type of platform poses several challenges that must be adequately tackled through control design: time-varying propellant sloshing, low control effectiveness, strong interactions between control loops, Thrust Vector Control (TVC) and guidance frequencies, as well as dynamical perturbations such as model uncertainties and atmospheric turbulence, which are critical for any launch vehicle [2].

DOI: 10.13009/EUCASS2022-4480

2 ADAMP control strategy

One key aspect to take into account in the design of a demonstrator platform like ADAMP demonstrator is its controllability. Essentially, one has to ensure that at all times along all typical missions of the vehicle and across its entire life span, the systems in charge of keeping the system under control are functioning well within their maximum performance capability. Given the maximum capabilities of the systems on the vehicle, its mission has to be designed in such way to ensure controllability. Currently, the ADAMP demonstrator is equipped with three major systems:
1. Rocket engine – responsible of controlling the altitude of the vehicle (vertical motion).
2. Thrust vectoring control system – responsible of controlling the pitch and implicitly the lateral motion of the vehicle.
3. Reaction control system – responsible for controlling the attitude of the vehicle with respect to its symmetry axis (roll).

Given the nature of missions that the ADAMP demonstrator is designed for, the design of the control system is based on a local horizontal reference frame, having its origin on the launch pad. The x axis will be oriented upwards, the z axis will be oriented to local North direction while the remaining y axis will be oriented to local East direction. This reference frame is denoted as the LP frame. The attitude of the vehicle will be parameterized by Euler angles (1-2-3 convention), relating the LP frame (considered to be inertial) and the body-fixed frame, denoted as the B frame, depicted in Figure 1. The B frame has its origin in the centre of mass of the dry structure.

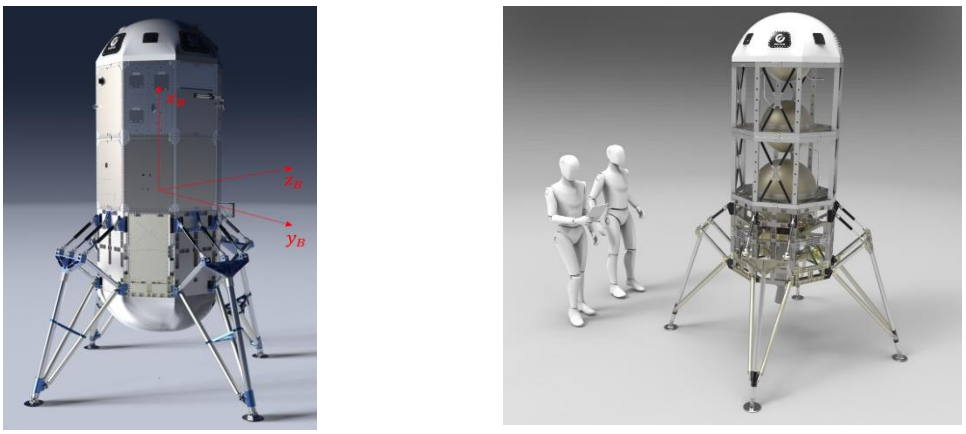

Figure 1 ADAMP Reference frames and relative size

The current control strategy for the ADAMP vehicle is based on a so-called divide-and-conquer approach. Essentially, separate controllers for position and attitude are designed and linked together in cascade-like fashion. Thus, following the scheme presented in Figure 2, a slower outer loop can be distinguished, responsible for controlling the position of the vehicle, and a faster inner loop, responsible for controlling the attitude. The outer loop is comprised of a set of two decoupled controllers, one for the vertical motion and one for the lateral motion. Low pass filters are used for noise influence reduction and sloshing suppression. The inner loop contains two separate controllers, one responsible for stabilizing the roll angle and/or the roll rate, and a second one responsible for the stabilization of the pitch and yaw angles (or simply denoted as pitch angles). The separation of controllers in the inner loop is motivated by the fact that commands corresponding to pitch and roll will be realized by different systems, i.e. the Thrust Vector Control (TVC) system for pitch and on-off gas thrusters for roll.

The command designed by the position controller consists of forces on the three axes of the LP frame. Based on these, under the assumption that the thrust is aligned with the symmetry axis of the vehicle, a thrust level command and an attitude command are issued and fed to the engine and the pitch controller, respectively. Following this approach, the thrust level realized by rocket engine is responsible for the vertical position, while the entire vehicle acts like an actuator for the lateral motion by pitching to corresponding direction. The command issued by the pitch controller consist of moment components on the y and z axes of the vehicle (B frame). Based on the thrust vector offset with respect to vehicle's the centre of mass, the required TVC deflections are derived.

For the control of the vehicle's roll motion, on-off cold gas thrusters are considered. For this reason, the roll controller will consist of a pulse modulator that will issue a pulse torque command that is further used to derive individual commands to the thrusters. Two pairs of thrusters are considered, one for each desired control torque direction.

Two sets of control methodologies were considered for the current project. The baseline methodology proposes linear controllers for position and pitch motion, designed in the means of H-infinity methods (Section 3). The second approach proposes position and pitch controllers based on nonlinear sliding mode control methodology (Section 4). A Schmitt Trigger relay was considered for roll angle and roll rate regulation (Section 5).

DOI: 10.13009/EUCASS2022-4480

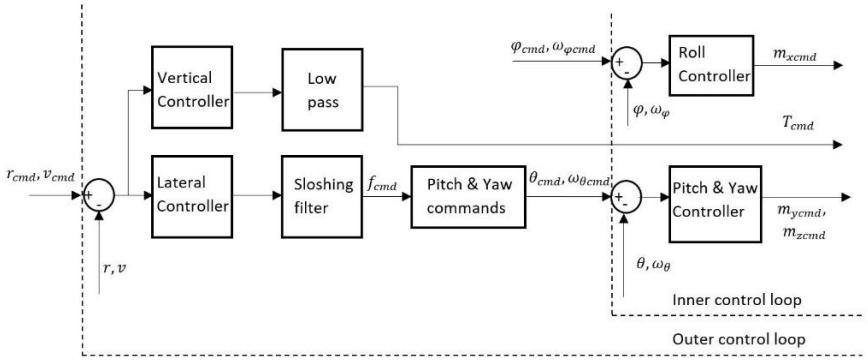

Figure 2 Control architecture

3 Structured H-infinity control system design

The control system design is divided into three main parts depending on the relevant vehicle dynamics considered in the process, the different systems controlling the respective channels or the methodology employed in the design. Thus, for the vertical translational motion of the vehicle (on the x axis of the LP frame) a rigid body plant model will be employed, neglecting the influence of aerodynamics and vertical sloshing modes of the liquid. The vertical channel (altitude) will be controlled by the thrust level realized by the rocket engine on the vehicle (Section 3.1).

The controllers for the lateral and pitch motion will be designed in a coupled manner due to the fact that strong couplings exist between respective channels and the lateral sloshing modes of the liquid in the two spherical tanks of the vehicle. The first sloshing modes will be taken into account in the control system design by employing a simple pendulum for each tank. The lateral and pitch motion will be controlled by TVC system on the vehicle (Section 3.2).

H-infinity synthesis is a frequency domain robust control method that was developed in the eighties and it is based on the use of H-infinity norm which measure the maximal value of the energy transmitted by a system. The method is applicable for MIMO, LTI, causal and proper systems and guarantees nominal stability, nominal performance and robust stability [3]. Unlike *traditional H-infinity* synthesis, which designs a full-order centralized controller with no possibility of imposing any structure, *structured H-infinity* synthesis approach allows to performed a H-infinity-based design by fixing the order and the structure of the controller. Other advantages of structured H-infinity synthesis include the direct quantification of stability and performance requirements in simple weighting functions and the use of Soft/Hard constraints enabling the automatic minimization of loads and consumption requirements ([3], [4], [5]).

3.1 Vertical controller

The dynamics for the vertical control system design (with respect to the LP frame) are simply (denoted as G_v):

$$m\ddot{r} = F_u - mg + F_d\,, \tag{3-1}$$

where m, F_u, F_d and g are vehicle mass, control force, disturbance force and gravitational acceleration, respectively. For controller design, the additive gravitational term will be neglected since it will be simply added to the controller output. In state space form, the equations are:

$$\begin{gathered} \dot{\boldsymbol{x}} = \boldsymbol{A}\boldsymbol{x} + \boldsymbol{B}\boldsymbol{u}\,, \\ \boldsymbol{y} = \boldsymbol{C}\boldsymbol{x} + \boldsymbol{D}\boldsymbol{u}\,, \\ \boldsymbol{A} = \begin{bmatrix} 0 & 1 \\ 0 & 0 \end{bmatrix},\quad \boldsymbol{B} = \begin{bmatrix} 0 & 0 \\ \frac{1}{m} & \frac{F_{dmax}}{m} \end{bmatrix},\quad \boldsymbol{C} = \boldsymbol{I}_2,\quad \boldsymbol{D} = \boldsymbol{0}_{2x2}\,, \\ \boldsymbol{x} = [r \quad v]^T,\quad \boldsymbol{u} = [F_u \quad F_d]^T. \end{gathered} \tag{3-2}$$

The engine responsible for generating the control force is modelled as a second order transfer function G_e, parameterized by gain K, natural frequency ω and damping ratio ζ:

$$G_e = K\frac{\omega^2}{s^2 + 2\,\zeta\omega s + \omega^2}. \tag{3-3}$$

where s represents the Laplace variable. In the equations above, the disturbance force that enters the system was scaled to be between 0 and 1 through the maximum disturbance F_{dmax}, considered to be 200 N. The states in the linear model

DOI: 10.13009/EUCASS2022-4480

are position r and velocity v. In order to take into account the mass variation of the system, a number of 10 operating points were defined, parameterized by mass. The mass considered for control system design ranged from 351 kg, corresponding to 1% fuel fill percentage, to 588 kg, corresponding to 99% fuel fill percentage. Correspondingly, a plant model was defined for each operating point. Parameters of the plant model considered for vertical control system design are depicted in Table 1.

Table 1 Plant parameters for vertical control design

	Nominal value	**Uncertainty**
Mass	351 – 588 kg	10 %
Engine gain	1.0	10 %
Engine natural frequency	2.5 rad/s	20 %
Engine damping ratio	0.65	20 %

The Robust Control Toolbox available in MATLAB [6] was employed for controller design. In this regard, a Linear Fractional Transformation (LFT) of the uncertain closed loop system was constructed for each operating point, consisting of a controller K_{vert}, the plant model G_v and the engine dynamics G_e presented above.
The controller consists of a combination of proportional, integrative and derivative gains and a low pass filter to reduce the effect of noise in the system. The controller output is given by:

$$F_u = \left[K_{pv}(m) + K_{iv}(m)\frac{1}{s}\right]\frac{K'}{K_f s + 1} + m(g + a_{cmd}) \,, \tag{3-4}$$

with

$$K' = K_{pr}(m)(r_{cmd} - r) + (v_{cmd} - v) \,.$$

Notice that the commanded acceleration a_{cmd} is also fed into the control law in order to achieve faster response to velocity changes and hence more accurate tracking.

In the controller architecture, K_{pr}, K_{pv} and K_{iv} were considered tunable parameters that are function of the system's mass. To achieve smooth transfer between operating points, gain surfaces were actually considered for tuning. Each gain was parameterized using a second order polynomial of the form:

$$K(m) = a_0 + a_1 m + a_2 m^2. \tag{3-5}$$

Notice that in this case the parameters a_n are the actual tunable parameters, thus reducing significantly the tuning effort. The filter time constant K_f was fixed to a value of 0.1.
A H-Infinity method implemented within *systune* framework in MATLAB was employed for tuning the gain surfaces of the controller. Requirements used in the tuning process are as following:

1. *Control force limitation* – maximum gain from the command r_{cmd} to controller output F_u was set to 1000 to avoid saturation.
2. *Wind disturbance rejection* – 20 dB/decade roll off with a bandwidth of 0.2 rad/s was imposed to the transfer between the disturbance F_d and the plant output r. Essentially, maximum gain was set to $s/0.2$, where s is the Laplace variable.
3. *Tracking error* – maximum 20% overshoot and maximum 1% DC error imposed to the transfer between command r_{cmd} and plant output r.
4. *Tracking bandwidth* – 0.3 rad/s imposed to the transfer between command r_{cmd} and plant output r. Currently, the bandwidth was selected such it is sufficiently lower than the rocket engine bandwidth, expected to be between 1.5 and 2 rad/s.
5. *Noise influence reduction* – imposed a priori through the filter parameter $K_f = 0.1$.

Figure 3 and Figure 4 depict the closed loop response to a step command and the corresponding control force for the designed controller. A good disturbance rejection capability is shown in Figure 5, where the response to a step disturbance is depicted.
Stability of the closed loop system was analysed using classical and disk margins, with emphasis on the plant input (the control force Fu). Values of between 5.8 and 6.3 dB disk gain margin and between 36 and 38 deg disk phase margin are obtained across all operating points, with variations of ±3 dB and ±10 deg on a span of 1000 samples of the uncertain closed loop system. Robust stability of the closed loop system was assessed by computing the μ structured singular value using the *robstab* function from MATLAB Robust Control Toolbox. Variation of the μ bounds with frequency is similar for all operating points and for simplicity only one operating point is shown in Figure 6. The closed

DOI: 10.13009/EUCASS2022-4480

loop system is found to be robustly stable in the presence of uncertainty since both lower and upper bounds of μ are well under the critical value of 1.

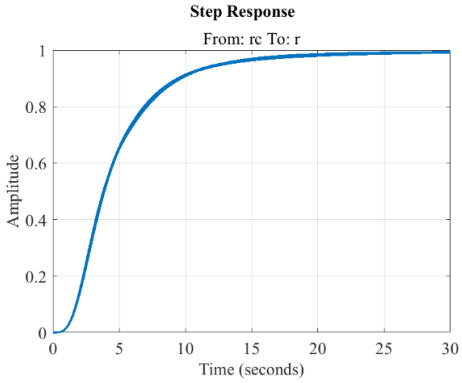

Figure 3 Closed loop step response (nominal)

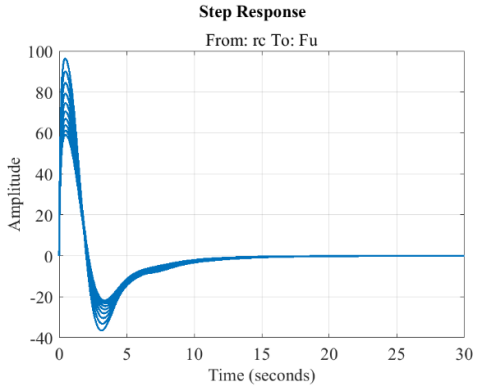

Figure 4 Control force for a step command (nominal)

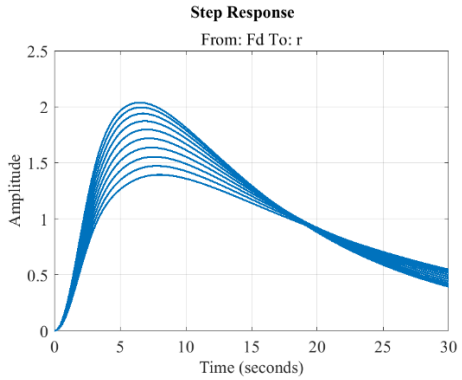

Figure 5 Closed Loop response to step disturbance (nominal)

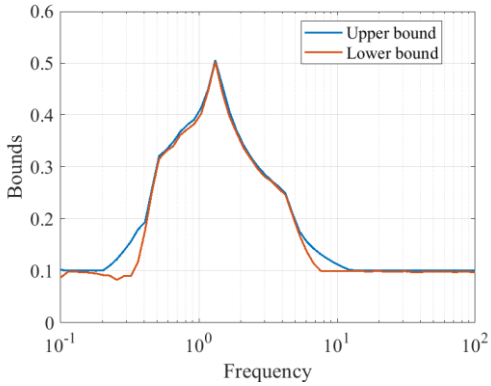

Figure 6 μ structured singular value bounds

3.2 Lateral and pitch/yaw controller

The plant model employed for lateral and pitch controllers design is depicted in Figure 7. Degrees of freedom to be controlled are in this case the lateral position r (in the LP frame, LP subscript neglected) and the pitch angle θ. Notice that the plant model is constructed on the hypothesis that the two lateral and pitch channels and the two sloshing channels for each tank are decoupled from each other. Following this approach, the designed lateral and pitch controllers will be applied similarly to remaining channels. The plant model in Figure 7 is described by the following:

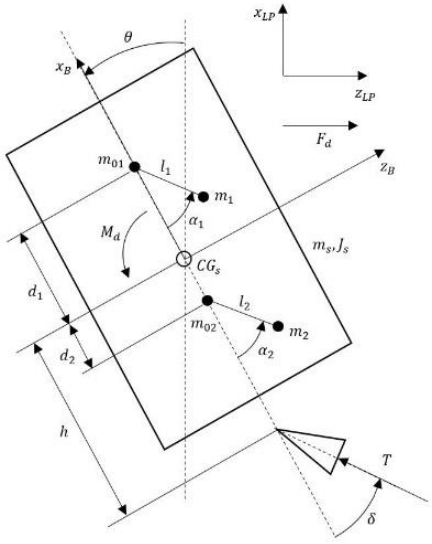

Figure 7 Plant model for lateral and pitch/yaw control design

DOI: 10.13009/EUCASS2022-4480

1. Degrees of freedom (states)
- r, θ – lateral position and pitch;
- α_1, α_2 – sloshing modes.
2. System inputs
- δ – TVC deflection;
- F_d – disturbance force;
- M_d – disturbance torque.
3. Constant parameters
- h, d_1, d_2 – TVC lever arm and tank center locations, respectively. Notice that these are measured with respect to the centre of mass of the dry structure CG_s hence the reason why they are constant. The tank locations are considered negative if the tank is located under the structural centre of mass.
- m_s, J_s – the mass and inertia of the dry structure.
4. Variable parameters
- $m_{01}, m_1, l_1, \zeta_1$ – rigidly attached mass, pendulum mass, pendulum length and viscous damping ratio for the upper tank (fuel tank);
- $m_{02}, m_2, l_2, \zeta_2$ – rigidly attached mass, pendulum mass, pendulum length and viscous damping ratio for the lower tank (oxidizer tank);
- T - thrust level.

As for the vertical motion, the aerodynamics are neglected and only disturbance force and torque will be considered in the model with maximum values of 200 N and 100 Nm, respectively. The equations of motion in state space form for the plant in Figure 7 are the following (denoted as G_L):

- State space form

$$\begin{gathered}\dot{\boldsymbol{x}} = \boldsymbol{A}\boldsymbol{x} + \boldsymbol{B}\boldsymbol{u}\,,\\ \boldsymbol{y} = \boldsymbol{C}\boldsymbol{x} + \boldsymbol{D}\boldsymbol{u}\,,\\ \boldsymbol{C} = \boldsymbol{I}_8,\ D = \boldsymbol{0}_{8x3}\,,\\ \boldsymbol{x} = [r \quad \theta \quad \alpha_1 \quad \alpha_2 \quad v \quad \dot{\theta} \quad \dot{\alpha_1} \quad \dot{\alpha_2}]^T,\ \boldsymbol{u} = [\delta \quad F_d \quad M_d]^T.\end{gathered} \tag{3-6}$$

- $\boldsymbol{A}$ matrix

$$m = m_s + m_{01} + m_{02} + m_1 + m_2, \qquad J = J_s + m_{01}{d_1}^2 + m_{02}{d_2}^2,$$
$$\boldsymbol{A} = \begin{bmatrix} \boldsymbol{N}_{11} & \boldsymbol{N}_{12} \\ \boldsymbol{H}^{-1}[\boldsymbol{N}_{21} & \boldsymbol{N}_{22}] \end{bmatrix}, \qquad \boldsymbol{N}_{11} = \boldsymbol{0}_{4x4}, \qquad \boldsymbol{N}_{12} = \boldsymbol{I}_{4x4},$$
$$\boldsymbol{N}_{21} = \frac{T}{m}\begin{bmatrix} 0 & n_{52} & 0 & 0 \\ 0 & n_{62} & 0 & 0 \\ 0 & n_{72} & n_{73} & 0 \\ 0 & n_{82} & 0 & n_{84} \end{bmatrix}, \qquad \boldsymbol{N}_{22} = \begin{bmatrix} 0 & 0 & 0 & 0 \\ 0 & 0 & 0 & 0 \\ 0 & 0 & n_{77} & 0 \\ 0 & 0 & 0 & n_{88} \end{bmatrix},$$
$$n_{52} = -m, \qquad n_{62} = (m_1 + m_{01})d_1 + (m_2 + m_{02})d_2\,,$$
$$n_{72} = n_{73} = -m_1 l_1, \qquad n_{82} = n_{84} = -m_2 l_2\,,$$
$$n_{77} = -2\zeta_1 m_1 l_1^2\sqrt{\frac{T}{m l_1}}, \qquad n_{88} = -2\zeta_2 m_2 l_2^2\sqrt{\frac{T}{m l_2}},$$

with the $\boldsymbol{H}$ matrix given by

$$h_{11} = m, \qquad h_{12} = m_1(l_1 - d_1) + m_2(l_2 - d_2) - m_{01}d_1 - m_{02}d_2\,,$$
$$h_{13} = m_1 l_1, \qquad h_{14} = m_2 l_2\,,$$
$$h_{21} = -d_1(m_1 + m_{01}) - d_2(m_2 + m_{02}), \qquad h_{22} = J + m_1 d_1(d_1 - l_1) + m_2 d_2(d_2 - l_2)\,,$$
$$h_{23} = -m_1 d_1 l_1, \qquad h_{24} = -m_2 d_2 l_2\,,$$
$$h_{31} = m_1 l_1, \qquad h_{32} = m_1 l_1(l_1 - d_1), \qquad h_{33} = m_1 l_1^2, \qquad h_{34} = 0\,,$$
$$h_{41} = m_2 l_2, \qquad h_{42} = m_2 l_2(l_2 - d_2), \qquad h_{43} = 0, \qquad h_{44} = m_2 l_2^2\,.$$

- $\boldsymbol{B}$ matrix

$$\boldsymbol{B} = \begin{bmatrix} \boldsymbol{P}_{11} \\ \boldsymbol{H}^{-1}\boldsymbol{P}_{21} \end{bmatrix},$$

DOI: 10.13009/EUCASS2022-4480

$$\boldsymbol{P}_{11} = \mathbf{0}_{4x4}, \quad \boldsymbol{P}_{21} = \begin{bmatrix} -T & F_{dmax} & 0 \\ -Th & 0 & M_{dmax} \\ 0 & 0 & 0 \\ 0 & 0 & 0 \end{bmatrix}.$$

The TVC responsible for generating the control torque is modelled as a second order transfer function G_{TVC}, parameterized by gain K, natural frequency ω and damping ratio ζ:

$$G_{TVC} = K \frac{\omega^2}{s^2 + 2\,\zeta\omega s + \omega^2}. \tag{3-7}$$

In order to take into account the variation of the plant dynamics, operating points parameterized by total mass and thrust level were defined. A total of 10 mass values along vehicle's mission, ranging from 380 kg to 588 kg, and 10 values for the thrust level, ranging from 2 to 6 kN, were considered. Consequently, a plant model was defined for each operating point. Notice that a mass reserve of approximately 30 kg is considered here (above the dry mass which is 350 kg), consisting of 22.5 kg of oxidizer and 7.5 kg of fuel (scaled approximately in accordance with mixture ratio).

Uncertainty in the plant model was introduced through its fixed parameters, scheduling variables and sloshing parameters. Uncertainty in the mass was reflected in the model through the dry mass and sloshing parameters, namely the rigidly attached masses m_{01} and m_{02}, and pendulum masses m_1 and m_2. Different uncertainty levels were considered for the sloshing parameters depending on the operating point. Due to space limitations, these will not be shown and discussed in this paper. The fixed parameters of the plant are depicted in Table 2.

Table 2 Plant parameters for lateral control design

	Nominal value	**Uncertainty**
Dry mass, m_s	350 kg	5%
Dry inertia, J_s	240 kgm^2	10%
Thrust level, T	from operating point	10%
TVC lever arm, h	0.72 m	±0.03 m
Fuel tank location, d_1	0.39 m	±0.03 m
Oxidizer tank location, d_2	-0.245 m	±0.03 m
TVC gain	1.0	5%
TVC natural frequency	67.8 rad/s	20%
TVC damping ratio	0.67	20%

In order to avoid resonance with the sloshing modes, a 10th order low pass filter was designed, consisting of two second order notch filters placed at the estimated bounds of sloshing frequencies (first modes, as modelled by the equivalent pendulum), denoted by ω_1 and ω_2, and a 6th order low pass filter. Here, oxidizer frequency bounds are used since the fuel frequency is slightly higher (due to lower size tank), thus ensuring attenuation of oscillations associated with both tanks. Intuitively, attenuation of higher sloshing modes is also implied. The transfer function of the resulting low pass filter is:

$$K_s = \frac{s^2 + 2g_1\zeta_1\omega_1 s + \omega_1^2}{s^2 + 2\zeta_1\omega_1 s + \omega_1^2} \frac{s^2 + 2g_2\zeta_2\omega_2 s + \omega_2^2}{s^2 + 2\zeta_2\omega_2 s + \omega_2^2} \left(\frac{\varepsilon s^2 + 2\eta\omega s + \omega^2}{s^2 + 2\eta\omega s + \omega^2} \right)^3, \tag{3-8}$$

with the following parameters:

- g_1 and g_2, controlling the amount of attenuation of the two notch filters;
- ζ_1 and ζ_2, controlling the width of the two notch filters;
- ω_1 and ω_2, the frequencies of the two notch filters;
- ε, controlling the amount of attenuation of the low pass filter;
- η and ω, controlling the roll off and bandwidth of the low pass filter.

As in the case of the plant model, the sloshing filter was gain scheduled with respect to mass and thrust level to ensure that maximum performance in terms phase delay and attenuation can be obtained. The tuning of the filter parameters was performed separately from the controller tuning, and was formulated as an NLP optimization problem that was solved using the *fmincon* solver in MATLAB. The bode diagram of the designed sloshing filter is shown in Figure 8.

DOI: 10.13009/EUCASS2022-4480

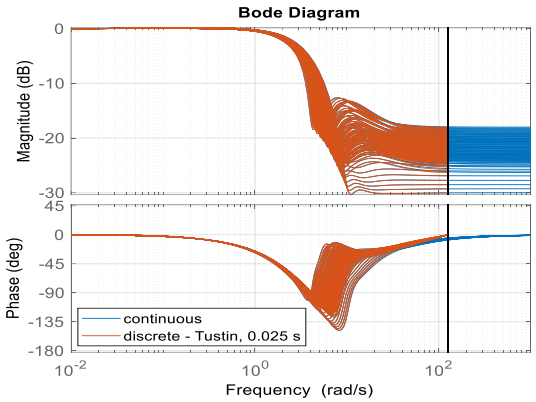

Figure 8 Bode diagram of the designed sloshing filter

The Robust Control Toolbox available in MATLAB was employed for controller design. In this regard, a LFT of the uncertain closed loop system presented in Figure 9 was constructed for each operating point, consisting of an outer control loop, responsible for the lateral control (through the controller K_{lat} and sloshing filter K_s), an inner control loop, responsible for pitch control (through the controller K_{pitch}) and the plant and TVC models G_L and G_{TVC} presented above. The block C in Figure 9 represents a coupling element computing pitch and pitch rate commands given the required lateral force F_u requested by the lateral controller K_{lat}. The commanded pitch and pitch rate are given by:

$$\theta_{cmd} = \frac{F_u}{T}, \qquad \omega_{cmd} = \frac{s}{0.1s+1}\frac{F_u}{T}. \tag{3-9}$$

For the lateral controller K_{lat}, the same architecture employed for the vertical controller was considered (3-4, without the gravitational term and the low pass filter), with the mention that the gains will be functions of mass and thrust level. The controller output is in this case:

$$F_u = \left[K_{pv}(m,T) + K_{iv}(m,T)\frac{1}{s}\right]K' + ma_{cmd}\,, \qquad K' = K_{pr}(m,T)(r_{cmd} - r) + (v_{cmd} - v)\,. \tag{3-10}$$

A simple PD architecture was used for the pitch controller. The pitch controller output is represented by the TVC deflection δ, given by:

$$\delta = K_{pt}(m,T)(\theta_{cmd} - \theta) + K_{po}(m,T)(\omega_{cmd} - \omega)\,. \tag{3-11}$$

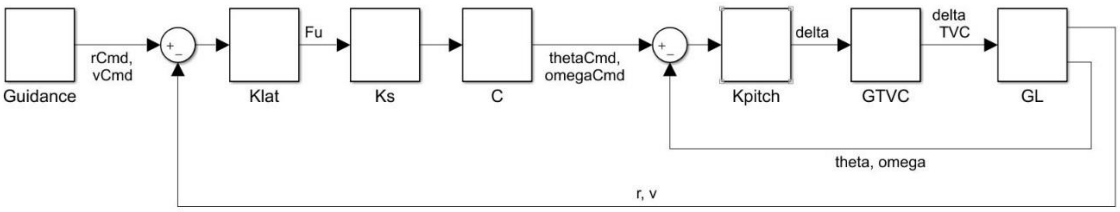

Figure 9 Closed loop system for lateral and pitch/yaw control design

To achieve smooth transfer between operating points, gain surfaces were considered for tuning. Each gain was parameterized using a second order polynomial of the form:

$$K(m,T) = a_0 + a_1 m + a_2 T + a_3 mT + a_4 m^2 + a_5 T^2. \tag{3-12}$$

A H-Infinity method implemented within *systune* framework in MATLAB was employed for tuning the gain surfaces of the controllers. Requirements used in the tuning process are as following:

- Inner loop (evaluated with open outer loop)
  1. *TVC actuation limitation* – maximum gain from the command θ_{cmd} to controller output δ was set to T_{max}/T, where T_{max} is the maximum available thrust and T is the thrust associated with the operating point of interest. This approach ensured that the same amount of control torque limitation is set for all operating points.
  2. *Tracking error* – maximum 20% overshoot and maximum 1% DC error imposed to the transfer between command θ_{cmd} and plant output θ.
  3. *Bandwidth* – 2.5 rad/s imposed to the transfer between command θ_{cmd} and plant output θ. Currently, the bandwidth was selected such it is significantly lower than the minimum sloshing frequency of 4.5 rad/s.
- Outer loop

DOI: 10.13009/EUCASS2022-4480

1. *Control force limitation* – maximum gain from the command r_{cmd} to controller output F_u was set to 1000 to limit the required pitch.
2. *Wind disturbance rejection* – 20 dB/decade roll off with a bandwidth of 0.2 rad/s was imposed to the transfer between the disturbance F_d and the plant output r. Essentially, maximum gain was set to $s/0.2$, where s is the Laplace variable.
3. *Tracking error* – maximum 20% overshoot and maximum 1% DC error imposed to the transfer between command r_{cmd} and plant output r.
4. *Bandwidth* – 0.3 rad/s imposed to the transfer between command r_{cmd} and plant output r. Currently, the bandwidth was selected such it is approximately one order of magnitude lower than inner loop bandwidth.
5. *Noise influence reduction* – implicitly managed by the sloshing filter.

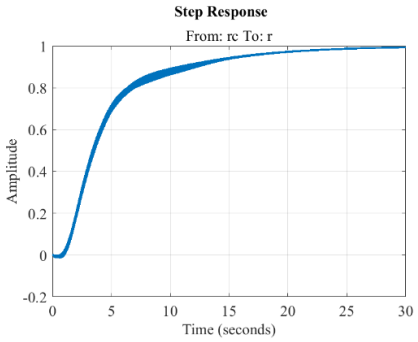

Figure 10 Lateral response to step command (nominal)

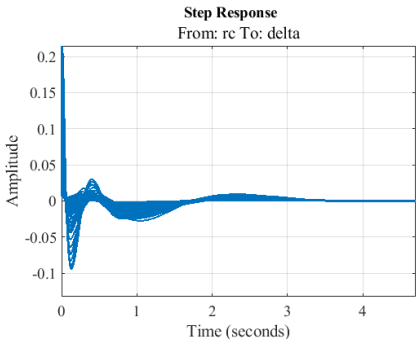

Figure 11 TVC response to lateral step command (nominal)

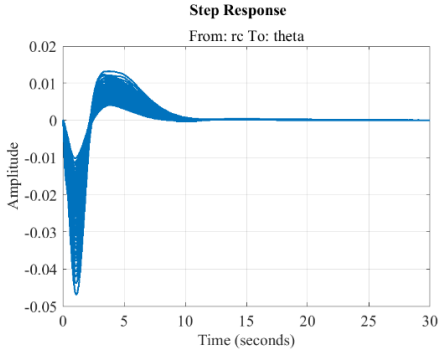

Figure 12 Pitch response to lateral step command (nominal)

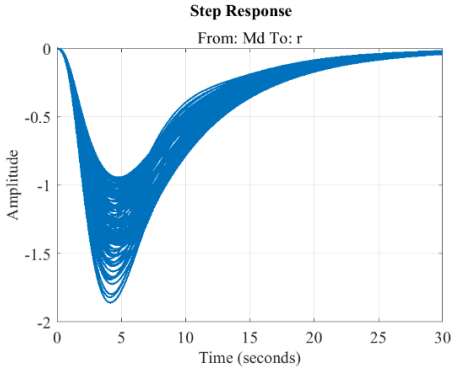

Figure 13 Position response to step torque disturbance (nominal)

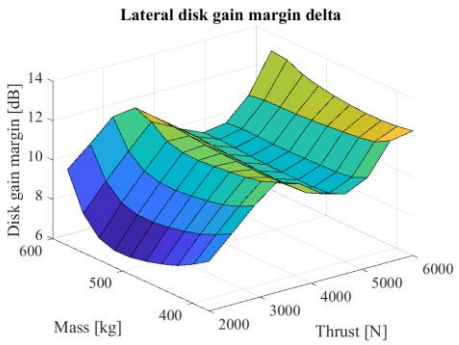

Figure 14 Disk gain margin at plant input as function of $\{m, T\}$

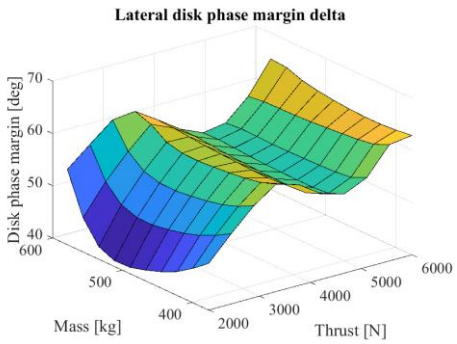

Figure 15 Disk phase margin at plant input as function of $\{m, T\}$

Figure 10 to Figure 12 depict closed loop response to a position step command and corresponding TVC actuation and pitch response. Very good attenuation of the sloshing behaviour is shown due to the presence of the sloshing filter in the outer control loop. A good disturbance rejection capability is also shown in Figure 13.

Stability of the closed loop system was analysed using classical and disk margins, with emphasis on the plant input (the TVC deflection δ). Figure 14 and Figure 15 depict disk gain and phase margins at the plant input for all operating points. Values between 6 and 14 dB were obtained for the gain margin and between 40 and 70 deg for the phase margin across the operating points, with variations of ±3 dB and ±10 deg on a span of 1000 samples of the uncertain closed loop system.

DOI: 10.13009/EUCASS2022-4480

4 Sliding mode control system design

A nonlinear control strategy was also implemented for ADAMP vehicle. Essentially, three nonlinear controllers were designed, one for each of the vertical, lateral and pitch channels. The approach allowed the simple replacement of the linear controllers from the already established control schemes for linear design, that is the K_{vert}, K_{lat} and K_{pitch} from equations 3-4, 3-10 and 3-11, respectively. The same sloshing filter developed in the latter section is kept in this nonlinear design. The vertical, lateral and pitch equations of motions used in the design are in vector form:

$$\ddot{\boldsymbol{x}} = \boldsymbol{f} + b_i u_i \,, \tag{4-1}$$

where $\boldsymbol{x}$ and $\boldsymbol{f}$ represent the states vector and the external forces and moments and are given by:

$$\begin{gathered} \boldsymbol{x} = [H \quad y \quad \theta]^T, \\ \boldsymbol{f} = \left[(F_x - mg + F_{dx})/m \quad \left(F_y + F_{dy}\right)/m \quad (M_z + M_{dz})/J\right]^T. \end{gathered} \tag{4-2}$$

In equations above, F_x, F_y and M_z are aerodynamic forces and moments, while m, J and g represent the mass of the vehicle, the moment of inertia and the gravitational acceleration, respectively. H, y and θ represent altitude, lateral position and pitch angle while $\boldsymbol{u}$ is the vector of control forces and moments, $\boldsymbol{u} = [u_H \quad u_y \quad u_\theta]^T$. F_{dx}, F_{dy} and M_{dz} are disturbance forces and moments while $\boldsymbol{b}$ is a gain vector given by:

$$\boldsymbol{b} = \left[\frac{1}{m} \quad \frac{1}{m} \quad \frac{1}{J}\right]^T. \tag{4-3}$$

The current control strategy is based on Slotine's work in [7], [8] and [9] related to sliding-mode control theory. Thus, for all three variables to track, we define corresponding sliding surfaces of the form:

$$s_i = \left(\frac{d}{dt} + \lambda_i\right)^{n-1} \int_0^t \tilde{x}_i d\tau = \dot{\tilde{x}}_i + 2\lambda_i \tilde{x}_i + {\lambda_i}^2 \int_0^t \tilde{x}_i d\tau \,, \qquad i = \{H, y, \theta\} \,, \tag{4-4}$$

where λ_i is a set of three positive constants, while n is the order of the dynamic system, in this case $n = 3$. The sliding surfaces s_i should not be confused with the Laplace variable from Section 3.The variables $\tilde{x}_i$ represent the tracking errors, i.e.:

$$\tilde{x}_i = x_i - x_{id} \,. \tag{4-5}$$

Notice that for good disturbance rejection, the variable of interest was chosen as the integral of the error hence why the order of the dynamic system is in fact 3. The controller design process is similar for all the three channels and for this reason the general approach is presented in the following by dropping the subscript i.

Looking more closely to equation 4-4, we notice that it represents a second order filter in variables $\tilde{x}$. Hence, we can state that the constant λ is nothing else than the break frequency of the filter, or the bandwidth of the close loop system. On a different interpretation, the equation $s = 0$ represents a hyperplane in the space $[\tilde{x} \quad \dot{\tilde{x}}]$, hence the terminology 'sliding surface'.

In order to ensure the global stability of the system for any $t > 0$, we are interested in finding a Lyapunov-like function $V(s)$, having the following properties:

$$\begin{cases} \lim\limits_{s\to\infty} V(s) \to \infty \\ V(s) > 0, \forall s \neq 0 \\ \dot{V}(s) < 0, \forall s \neq 0 \end{cases}. \tag{4-6}$$

If such function exists, the variable s will always tend to 0, and the system will be asymptotically stable. Adequate candidate function in this case is given by:

$$V(s) = \frac{1}{2} s^2. \tag{4-7}$$

It is straight-forward to see that the first two conditions in 4-6 are easily satisfied. What remains to do is to find a suitable control law u, which will ensure that the third condition in 4-6 is satisfied for all $t > 0$, hence $V(s)$ remains a Lyapunov-like function for all $t > 0$. Moreover, this condition must be satisfied despite the presence of model imprecisions and uncertainties or external disturbances. For this reason, we must first have a mathematical description of the dynamic model imprecisions or disturbances. Let us assume that the function f is not exactly known, but estimated as $\hat{f}$. Assuming the estimation error on f is bounded by some known function $F(x, \dot{x})$, we can write

$$\left|\hat{f} - f\right| \leq F. \tag{4-8}$$

Also, let's assume that the control gain b is unknown but has known bounds, i.e.

$$0 < b_{min} \leq b \leq b_{max} \,. \tag{4-9}$$

Since the gain enters multiplicatively in the dynamic equations, it is more practical to define the bounds in the form

DOI: 10.13009/EUCASS2022-4480

$$\beta^{-1} \leq \frac{\hat{b}}{b} \leq \beta \,, \tag{4-10}$$

where β and the estimated gain $\hat{b}$ are given by

$$\beta = \sqrt{\frac{b_{max}}{b_{min}}}, \qquad \hat{b} = \sqrt{b_{min} b_{max}} \,. \tag{4-11}$$

The first step towards defining a control law that satisfies conditions 4-6, is to define a so-called equivalent control, or estimated control, that will keep the system in sliding mode ($\dot{s} = 0$) when its dynamic is exactly known. Thus, differentiating equation 4-4 and using 4-1, we can write

$$\dot{s} = f + bu - \ddot{x}_d + 2\lambda\dot{\tilde{x}} + \lambda^2\tilde{x} = 0 \,, \tag{4-12}$$

which further gives the estimated control law as:

$$\hat{u} = \frac{1}{\hat{b}}\left(-\hat{f} + \ddot{x}_d - 2\lambda\dot{\tilde{x}} - \lambda^2\tilde{x}\right) = \frac{\hat{u}_0}{\hat{b}} \,. \tag{4-13}$$

In order to ensure that conditions 4-6 are satisfied in the presence of uncertainty in the dynamics f and gain b, we add to $\hat{u}$ a discontinuous term across the surfaces $s = 0$:

$$u = \frac{1}{\hat{b}}[\hat{u}_0 - ksgn(s)] \,, \tag{4-14}$$

where k represents a positive gain and *sgn* is the sign function. To satisfy the third condition in 4-6, we impose

$$\frac{1}{2}\frac{d}{dt}(s^2) \leq -\eta|s| \,, \tag{4-15}$$

which further gives

$$\dot{s}s \leq -\eta|s| \,, \tag{4-16}$$

where η is a strictly positive constant. The above condition is called the *sliding condition*.

Essentially, it states that the 'distance' to the surface decreases along all system trajectories. That is, all the possible trajectories are constrained to point to the surface $s = 0$, and once on the surface to remain on it. Practically, the surface represents an *invariant set* for the dynamic system, denoting global stability. Using the control law in 4-14, and substituting in 4-16, we obtain after simple algebraic manipulations:

$$\left[f - \hat{f} + \left(\frac{b}{\hat{b}} - 1\right)\hat{u}_0\right]s - \frac{b}{\hat{b}}k|s| \leq -\eta|s| \,. \tag{4-17}$$

It is straight-forward to show that a gain that will satisfy the above condition is given by

$$k = \beta[F + \eta + (\beta - 1)|\hat{u}_0|] \,. \tag{4-18}$$

One of the most important drawbacks of the sliding-mode approach is known as *chattering*. This phenomenon is due to the term $-ksgn(s)$ in the control law, and leads to high control activity which may excite high frequencies dynamics and/or destroy the actuators. A smoother control law in the vicinity of the surface $s = 0$ can be obtained by replacing the *sign* function with the *saturation* function, i.e.

$$u = \frac{1}{\hat{b}}\left[\hat{u}_0 - ksat\left(\frac{s}{\delta}\right)\right], \qquad sat\left(\frac{s}{\delta}\right) = \begin{cases} sgn(s), & |s| > \delta \\ \dfrac{s}{\delta}, & |s| \leq \delta \end{cases} . \tag{4-19}$$

This will ensure that the contribution of the second term in the control law is damped in the vicinity of the surface, that is when $-\delta \leq s \leq \delta$, resulting in a smoother control action. The space where $-\delta \leq s \leq \delta$ is called *boundary layer* and δ represents a small positive number called the boundary layer *thickness*. Note that in these circumstances, the boundary layer becomes the invariant set for the dynamic system.

It is common practice that the system bandwidth λ is chosen to be small with respect with high frequency unmodelled dynamics of the system. Assuming the bandwidth is limited by the system's mechanical properties, we can find a measure of the order of magnitude for the thickness δ by writing the equation 4-12 in the boundary layer, i.e.

$$\dot{s} = -\frac{b}{\hat{b}}\left(\frac{k}{\delta}\right)s + e \,, \tag{4-20}$$

where e is some error term. It is easy to see that this represents a first order filter in the variable s. Imposing the condition that its break frequency be smaller or equal than the one of the filter in equation 4-4, and assuming gain k is upper bounded by some positive number k_{max}, we can select the boundary layer thickness to verify the equation

$$\lambda\delta = \beta k_{max} \,, \tag{4-21}$$

DOI: 10.13009/EUCASS2022-4480

which is denoted as the *static balance condition*. The above condition represents a trade-off between robustness and tracking precision. This can be further improved by allowing the thickness δ to be time-dependent. In this case, in order to maintain the boundary layer attractiveness, the condition 4-16 is replaced by

$$\dot{s}s \leq \left(\dot{\delta} - \eta\right)|s| \,. \tag{4-22}$$

Following the same procedure as above, we can show that the gain k in the control law 4-19 is replaced by

$$\bar{k} = k - \beta\dot{\delta} \,. \tag{4-23}$$

Writing the dynamics of the variable s in the boundary layer as above, we can show that the boundary layer thickness is the output of the first order filter:

$$\dot{\delta} + \frac{1}{\beta^2}\lambda\delta = \frac{1}{\beta}k \,. \tag{4-24}$$

Finally, the implemented control law is given by:

$$u = \frac{1}{\hat{b}}\left[\hat{u}_0 - \bar{k}sat\left(\frac{s}{\delta}\right)\right]. \tag{4-25}$$

Robustness in the designed nonlinear controllers was introduced by directly embedding similar uncertainties as for the linear controllers into the bound function F in equation 4-8. Corresponding trade-off between robustness and tracking performance is being handled automatically through the boundary layer δ. Bandwidths of 0.4 rad/s and 2.5 rad/s were selected for the position controllers and pitch controller, respectively.

5 Roll control system design

There are two different needs for the roll control system on the ADAMP vehicle. The primary role of the RCS is to regulate the roll angle while keeping the angular rate within small bounds to ensure no significant coupling between roll and pitch channels. Another role of the RCS for missions where the angle regulation is not required is to simply regulate the roll rate to ensure pitch channels decoupling. For both cases, a nonlinear switching logic based on the Schmitt Trigger was implemented. The control architecture considered for roll angle regulation is depicted in Figure 16, consisting of a linear switching logic (controller), a pulse modulator (Schmitt Trigger), thrusters and a single axis ideal plant. For roll rate regulation, only the roll rate is fed to the Schmitt Trigger and its parameters are tuned based on maximum allowed roll rate and minimum pulse width. Further details regarding the subject are outside the scope of this paper.

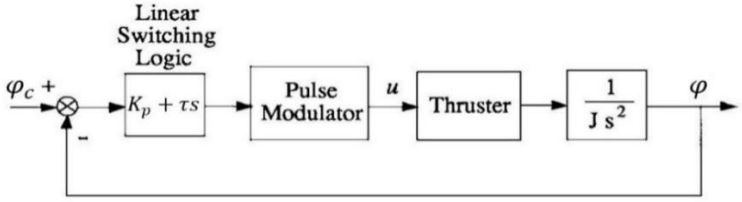

Figure 16 Single axis reaction control system (angle regulation)

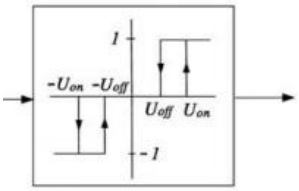

Figure 17 Schmitt Trigger

6 6DoF simulations

In order to test, analyse and validate the controller design in a realistic environment, a high fidelity 6DoF simulator was developed within the ADAMP project. The simulator was developed in the MATLAB-Simulink environment and some of its most important features include:

- Full set of 6DoF nonlinear equations of motion;
- Actuator models, including nonlinear effects such as setpoint and rate saturations, delays, dead bands, biases, etc.;
- An Inertial Navigation System (INS) model, including gyroscope and accelerometer models, GNSS receiver models and Attitude and Heading Reference System model (AHRS).
- Detailed environment modelling, including von Karman wind turbulence, discrete gust and wind shear models, NRLMSISE00 atmospheric model and J2 gravitational model;
- Nonlinear equivalent spherical pendulum sloshing model (modelling the first sloshing mode in the spherical thanks);
- Full 6DoF aerodynamic database;
- Monte Carlo Analysis, Sensitivity Analysis and Worst-Case Analysis capabilities.

DOI: 10.13009/EUCASS2022-4480

For the purpose of this work, a comparative study has been performed with the aim of analysing the relative performance of the two controller design approaches: the structured H-infinity from Section 3 and the sliding mode control (SMC) from Section 4. In this regard, an ascent and descent reference trajectory was considered, with a maximum altitude of around 600 m and a maximum velocity of 20 m/s. The reference trajectory was designed through means of trajectory optimization using an in-house tool developed for the purpose of the project. Reference position and velocity are depicted in Figure 18 and Figure 19, respectively.

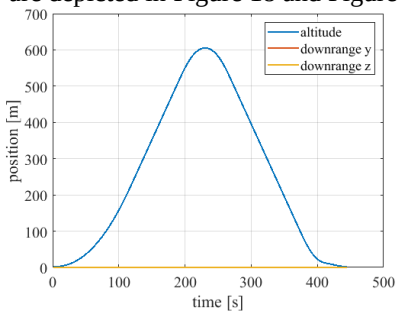

Figure 18 Reference trajectory

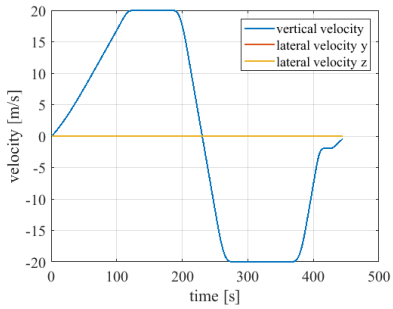

Figure 19 Reference velocity

The robustness of both baseline H-infinity control architecture and sliding mode control architecture was analysed in the presence of nonlinearities, parametric uncertainties and external disturbance within Monte Carlo simulations performed with the high fidelity 6DoF simulator. A total number of 10000 random trajectories were simulated for each of the two control architectures.

Figure 20 and Figure 21 depict the altitude tracking error for the two control architectures. Here, it can be seen that the sliding mode controller shows better tracking performance for the nominal mission, with maximum altitude error of 1.5 m, compared to an error of 4 m for the linear controller. However, a slightly higher degree of dispersion can be observed for the sliding mode controller on the span of all random trajectories, especially in the second half of the flight. Still, the sliding mode controller has a lower dispersion in the first half of the flight. The results suggest that some improvements are needed for the SMC to reach the robustness of the linear controller. For the lateral channel, the tracking errors are depicted in Figure 22 and Figure 23. As for vertical tracking, the sliding mode controller proves to be more performant when compared to the linear controller, with a maximum error of 1 m compared to an error of 2 m shown by the linear controller. However, on the span of all random trajectories, the tracking errors of the two controllers show similar dispersions, even though a few outliers show slightly higher errors for the sliding mode controller.

Figure 24 and Figure 25 show the pitch angle of the vehicle with respect to the local vertical. Naturally, the pitch angle results from the need to compensate for the lateral wind acting on the vehicle throughout the mission. It can be seen that both the nominal pitch angle profile and the degree of dispersion are similar for the two controllers, with maximum peak pitch angles of 20 degrees, at maximum lateral winds of 20-25 m/s. The corresponding TVC deflections are shown in Figure 26 and Figure 27. Here, similar nominal profiles and dispersions are shown for the two controllers, reaching a maximum deflection of 9 degrees out of a maximum capability of 14 degrees. It is worth noticing that most of the TVC deflection results from the need to compensate the static aerodynamic moment generated by the high lateral winds. Figure 28 and Figure 29 depict the engine thrust levels for the two controllers. As expected, similar nominal profiles and dispersions are shown for the two controllers, with now saturation of the maximum capability of 6.5 kN.

6.1 Summary

Both controllers seem to be a viable solution for ADAMP platform, however there are differences between them which can be synthetized in the table below:

Table 3 Comparison of structured H-infinity and sliding mode controllers

	Structured H-inf	Sliding Mode
Better nominal performance		✓
Good disturbance rejection capabilities	✓	✓
Better robustness (smaller dispersions)	✓	
Formal stability, robustness and worst-case analysis techniques	✓	
Configurable controller size & architecture	✓	✓
Introduction of nonlinear effects in the control law		✓
Easier handling of design requirements	✓	
Design effort		✓

DOI: 10.13009/EUCASS2022-4480

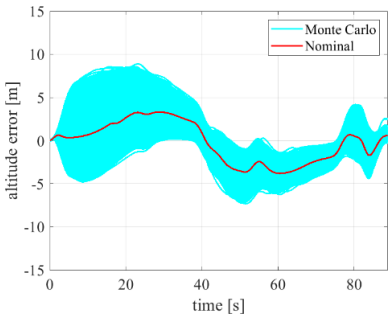

Figure 20 Altitude error (H-infinity)

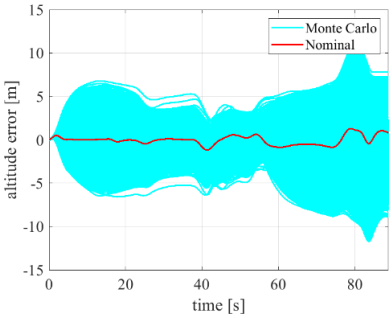

Figure 21 Altitude error (SMC)

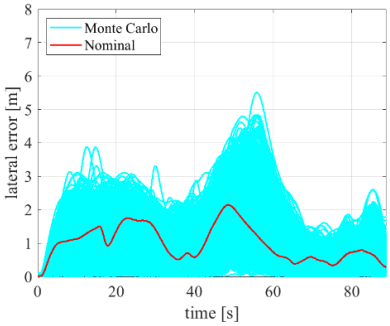

Figure 22 Lateral error (H-infinity)

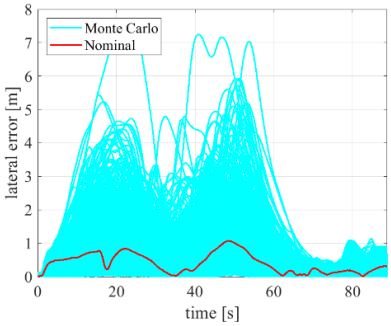

Figure 23 Lateral error (SMC)

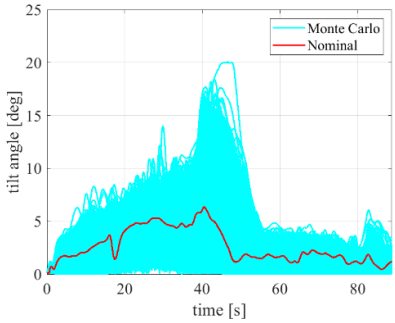

Figure 24 Pitch angle (H-infinity)

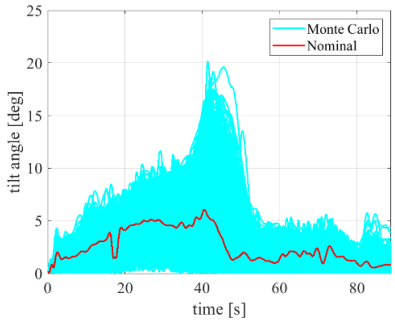

Figure 25 Pitch angle (SMC)

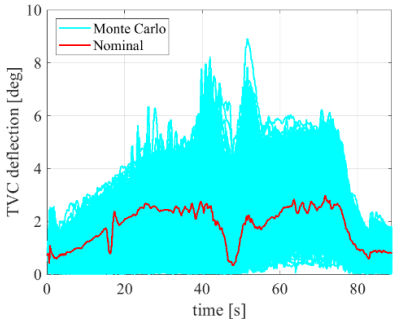

Figure 26 TVC deflection (H-infinity)

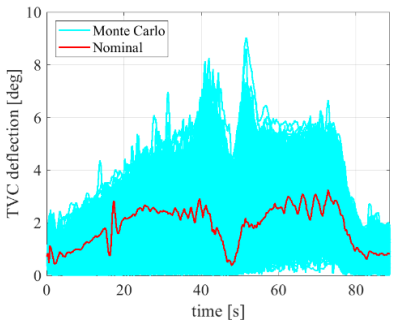

Figure 27 TVC deflection (SMC)

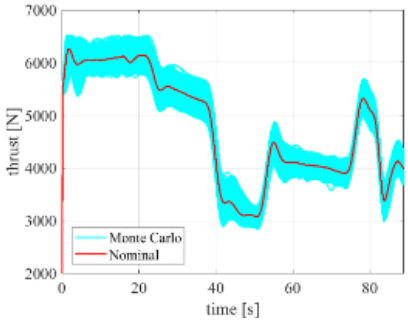

Figure 28 Thrust force (H-infinity)

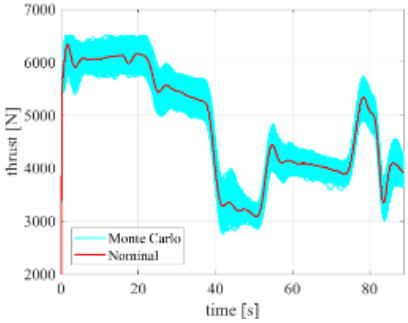

Figure 29 Thrust force (SMC)

DOI: 10.13009/EUCASS2022-4480

7 Conclusion

This paper discussed the control strategy adopted within the ADAMP project. Two control strategies were considered in the design. The baseline control strategy of the ADAMP vehicle is based on a structured H-infinity methodology. Throughout the paper, several aspects of the control system design were presented, including linear plant modelling, selected controller structure, controller tuning, classical stability, robust stability and sloshing filter design. The second control strategy considered in the design is based on a nonlinear sliding mode control methodology. This paper discusses in detail design process of control laws based on Lyapunov global stability theory as well as possibilities to ensure proper trade-offs between robustness and tracking performance, similar to what it is required for linear controller design through H-infinity methods.

A comparative study was performed in order to analyse the relative performance and robustness of the two control methods. An ascent and descent mission was selected for the study and a Monte Carlo analysis was performed within a high-fidelity 6DoF simulator for each of the two control architectures. The results showed comparable performance and robustness of the two control methods for the lateral control channel. On the other hand, H-infinity controller showed better robustness for the vertical control channel. It is worth noticing that the superiority of the H-infinity controller is all the more remarkable since no knowledge of vehicle aerodynamic properties was embedded into it, as opposed to the sliding mode controller. Nevertheless, the results are indicating that nonlinear sliding mode control methodology might be a viable alternative to the well proven linear control approach.

It is worth mentioning that a maturation on both controllers design will be done in the next project phase, as the results from the sub-system identification activities will be integrated in the Flight Simulator and their performances and robustness will be re-investigated.

8 Acknowledgement

This study and the ADAMP project are funded by the European Space Agency (ESA) through contract No. 4000130099/20/NL/CRS/hh. The authors would like to express their gratitude towards the Romanian Space Agency (ROSA) for their support, to ESA General Support Technology Programme (GSTP) Office and to Mr. David Perigo.

9 Bibliography

[1] A. Neculaescu, A. Marin and A. Toader, "System Identification and Testing for a VTVL vehicle," in *EUCASS Conference*, 2019.

[2] P. Simplicio, A. Marcos and S. Bennani, "New Control Functionalities for Launcher Load Relief in Ascent and Descent Flight," in *EUCASS Conference*, 2019.

[3] M. Ganet-Schoeller and J. Desmariaux, “Structure H-infinity sunthesis for flexible launcher control,” in *IFAC Hosting by Elsevier Ltd.* , 2016.

[4] D. Navarro-Tapia, A. Marcos, S. Bennani and C. Roux, "Structured H-infinity and Linear Parameter Varying Control Design for the VEGA Launch Vehicle," in *EUCASS*, 2017.

[5] P. Apkarian, M. Dao and D. Noll, "Parametric robust structured control design," *IEEE Trans. Automat. Control*, vol. 60, no. 7, pp. 1857-1869, 2015.

[6] G. Balas, R. Chiang, A. Packard and M. Safonov, “MATLAB Robust Control Toolbox User's Guide, third ed.,” Mathworks, 2006.

[7] J. Slotine and W. Li, Applied Nonlinear Control, Prentice-Hall, 1991.

[8] J. Slotine and S. Sastry, "Tracking control of non-linear systems using sliding surfaces, with application to robot manipulators," *International Journal of Control*, pp. 465-492, 1983.

[9] J. Slotine, "Sliding controller design for non-linear systems," *International Journal of Control*, pp. 421-434, 1984.